Gas Chromatography–Trapped Ion Mobility Mass Spectrometry: A Highly Specific and Ultra-Sensitive Platform for Quantifying Sub-ppt Levels of Dioxins and PCBs in Food

Hugo B. Muller, Georges Scholl and Gauthier Eppe

Mass Spectrometry Laboratory, University of Liège, 4000 Liège, Belgium

1. Introduction

Ion mobility spectrometry (IMS) is a technique that separates ions based on their transport properties in a buffer gas under the influence of an external electric field[1]. Although its origins trace back over a century, IMS began to emerge as a viable analytical tool in the 1970s[2]. Owing to its rapid analysis time, high sensitivity and portability, it was soon adopted as a standalone technique for the on-site detection of a wide range of analytes. To this day, IMS continues to be employed for the trace detection of compounds such as explosives[3], illegal drugs[4] and chemical warfare agents[5]. However, when used as a standalone device, IMS truly lacks selectivity. For this reason, the analysis of more complex samples by IMS has usually been performed through the coupling with complementary separation techniques such as gas chromatography[6,7] (GC-IMS) and, more recently, mass spectrometry[8] (IM-MS).

In the field of contaminants and pollutants analysis, the interest in IM-MS platforms is emerging and has been growing significantly in the last 5 years. Indeed, several studies have demonstrated the potential of IM as powerful additional technique to improve the analysis of both legacy and emerging contaminants[9,10]. They have highlighted three key advantages offered by the hyphenation of ion mobility to traditional LC and GC-MS workflows: 1) improvement of the peak capacity with the additional dimension of separation; 2) cleaner (tandem) mass spectra; and 3) more confident compound annotation using collision cross section (CCS) values. These assets have recently resulted in the publication of a number of applications where IM-MS is employed, often hyphenated with LC, for the analysis of a diverse range of contaminants[9,10]. However, while such applications have been mainly qualitative approaches, quantitative applications for pollutant compounds have been comparatively scarce.

Interestingly, some of the earliest reports of quantitative IM-MS applications, across all research fields, dated back to 1999-2000. Theses pioneers studies, conducted by the group of Guevremont, focused on the targeted analysis of disinfection by products (DBPs) such as perchlorate in water using a homebuilt FAIMS device hyphenated to a commercial LC-quadrupole[11–13]. Since then, only a few works have focused on the targeted analysis of contaminants such as per- and polyfluoroalkyl substances (PFAS)[14], organic micropollutants (OMPs)[15], hydroxylated polychlorobiphenyls (PCBs)[16], non-intentionally added substances (NIAS)[17], pesticides[18] and veterinary drug residues[19] have been published. Moreover, while promising preliminary quantitative performance results have been reported in these studies, a thorough validation of the performances of current IM-MS instrumentation for the quantitative analysis of trace contaminants, comparable to the efforts undertaken for other classes of small compounds such as metabolites[20–25], remains lacking.

To address this gap, the present study aimed at thoroughly evaluating the capabilities of a modern commercially available IM-MS instrument (timsTOF pro 2 from Bruker) to accurately quantify trace amounts of well-known legacy contaminants, the dioxins and the PCBs, in food samples. Traditional targeted analytical methods for these compounds, such as gas chromatography coupled with high-resolution sector mass spectrometry (GC-HRMS)[26] or triple quadrupole MS[27] operated in selected or multiple reaction monitoring (SIM or MRM), offer high sensitivity and specificity. However, these techniques can be challenged by isobaric matrix interferences[28] and, in the case of GC-sector HRMS, still the current gold standard method, require complex maintenance and highly trained personnel[29]. The integration of ion mobility separation has the potential to enhance method selectivity by increasing peak capacity, similar to multidimensional gas chromatography approaches[30].

In this study, three fat samples (fish oil, palm oil and milk fat) from proficiency tests (PTs) were analyzed on a GC-APCI-TIMS-MS device. After method optimization, analytical performance was assessed in accordance with Commission Regulation (EU) 2017/644 and compared with the reference confirmatory method for dioxins and PCBs, the GC–EI–sector HRMS. The potential benefits of ion mobility, particularly in terms of improved selectivity and peak capacity, are further discussed in the final section of the paper.

2. Experimental

2.1 Chemicals

All congeners of PCDD/Fs (the seventeen 2,3,7,8-substituted), non-ortho (NO-)PCBs (PCBs 77, 81, 126, 169), mono-ortho (MO-)PCBs (PCBs 105, 114, 118, 123, 156, 157, 167, 189) and NDL indicator PCBs (PCBs 28, 52, 101, 138, 153, 180) were

quantitated against their own 13C-labeled internal standards according to the isotopic dilution method. Native and 13C-labelled standards were purchased from Wellington Laboratories (Ontario, Canada). For the calibration curves, 6 level calibration solutions were prepared for the PCDD/Fs and the NO-PCBs, 8 for the MO-PCBs and 9 for the NDL-PCBs. The detailed concentrations for each calibration level are given in Tables S1. Recovery rates were checked with recovery standards (1,2,3,4-TCDD for PCDD/Fs and PCB 80 for PCBs). All solvents used were of the highest purity, suitable for the analysis of trace contaminants (Biosolve, Dieuze, France).

Besides, a standard mixtures of 20 PBDEs was purchased from Wellington and used to optimize certain specific method parameters (see dedicated sections in the main text). The rationale behind the decision to utilise PBDEs instead of PCBs or PCDD/Fs for this particular objective is that PBDEs encompass a more extensive range of m/z and ion mobilities, thereby ensuring greater generalisability of the outcomes.

2.2 Sample preparation

The oil fat samples analysed in this study were aliquots of PT samples provided by the European Reference Laboratory for Dioxins and PCBs in Food and Feed (EU-RL, Freiburg, Germany). The three matrices were fish oil (EURL-PT-DP_1601-HF), palm oil (EURL-PT-DP_1701-PF) and milk fat (EURL-PT-DP_1302-MI). These matrices were chosen because they required the same sample preparation procedure and because their profile and level of contamination were different.

The sample preparation was performed according to our ISO17025 accredited protocol for the analysis of PCDD/Fs and PCBs in foodstuffs. Briefly, each fat samples (2g for fish oil; 4g for palm oil and milk fat) were dissolved in a mix of 14 mL *n*-hexane and 1 mL of toluene, spiked with 13C-labeled internal standards and then loaded on an automated Dextech Heat system (LCTech, Germany) for multiple column clean-up and fractionation. The samples in hexane were sequentially eluted through $AgNO_3$, H_2SO_4, and KOH supported on silica and basic alumina for lipid breakdown and removal of some interferences. Then, on an activated carbon column, two fractions were collected, a first one with non-planar congeners (MO- and NDL-PCBs, referred to in this text as the "PCBs fraction") and a second one with the planar congeners (PCDD/Fs and NO-PCBs, referred to as the "dioxins fraction"). These fractions were then transferred to GC vials containing *n*-Nonane as keeper solvent, evaporated under a gentle stream of nitrogen and finally spiked with the recovery standards before analysis. The final volumes were 100 and 9 μL for the PCBs and dioxins fraction, respectively. For each matrix, two sets of six aliquots were taken and prepared according to the abovementioned protocol (one set for GC-TIMS-TOFMS and the other for GC-sectorHRMS). A total of 10 procedural blanks were also prepared in parallel. All the sample preparation was performed by qualified and experienced technicians from our routine trace contaminants laboratory.

2.3 Instrumentation

2.3.1 GC-APCI-TIMS-TOFMS

Measurements were performed on a commercial timsTOF Pro 2 mass spectrometer (Bruker, Bremen) equipped with a Scion 456-GC connected to an atmospheric pressure chemical ionization (APCI) source for sample introduction and ionization (GC-APCI II, Bruker, Bremen).

Injections were conducted in splitless mode (injection temperature 275 °C, 1 µL) for the PCBs fraction (MO- and NDL-PCBs) and in solvent vent PTV mode (injection temperature 80 °C, 5 µL) for the dioxins fraction (PCDD/Fs and NO-PCBs). The GC column was a low polarity Rxi-5Sil MS column (30 m × 0.25 mm × 0.25 µm, Restek). Helium (grade 6.0, Air Liquide, Belgium) was used as the carrier gas. More details about the GC conditions are given in Table S2.

Analytes were ionized in positive APCI mode and were generated mostly as stable radical molecular ions $M^{+\cdot}$, along with a small proportion of protonated $[M+H]^+$ ions (a detailed list of the ionization source parameters used is provided in Table S3).

Ion mobility separations were performed by trapped ion mobility (TIMS). In this technique, a combination of electric field gradient and fast moving gas is used to trap and then elute the ions toward the mass spectrometer by order of increasing ion mobility coefficient (i.e., decreasing CCS). It is a versatile IM technology that can provide high resolution separations (R_p > 100) and duty cycle (up to 100%). More details about the basic principles of TIMS are available elsewhere[31,32]. A complete list of the optimized parameters used in this study (voltages, pressure, analysis times, etc.) is provided in Table S4. The TIMS separations were performed in SWIM mode. This concept was introduced in one of our previous work[33] and enables to significantly increase the IM resolving power for chromatography hyphenated TIMS applications. More details about the application of SWIM to the analysis of both fractions are given in Figure S1. The resolving power achieved varied roughly between 100 and 220 depending on the quantity of analyte injected (1 to 500 pg, Figure S2). The optimization of the accumulation time is further discussed in a dedicated part of the results and discussion section. Ion mobility calibration was performed according to our previously developed procedure using siloxane ions from the GC column bleed[33] (Table S5).

Calibrated CCS values of the targeted compounds are presented in Table S6. The qTOF analyzer was operated at 10 kHz in the range m/z 100−1000 in MS only mode (additional parameters are provided in Table S7). Mass calibration was performed using siloxane ions (Table S5).

2.3.2 GC-sectorHRMS

Reference measurements were performed on an Autospec sector mass spectrometer (Waters, Manchester, UK) coupled to an Agilent 7890 gas chromatograph (Palo-Alto, CA, USA). The GC conditions were similar to the injections performed on the timsTOF instrument, with the exception of the GC columns which were different (a 50m J&W VF-5ms column for the dioxins fraction and a 25m Trajan HT8 column for the PCBs fraction). The ionization was performed in electron impact (EI) at 35 eV. The mass resolving power was set to 10 000 (10% valley definition) in single ion monitoring (SIM) mode.

2.4 Data treatment

For the GC-timsTOFMS analysis, data processing was performed using the software Data-Analysis (Bruker, version 5.3). Two approaches of peak integration were considered: quantitation based on the areas of the ion mobility peaks or quantitation based on the areas of the IM-filtered chromatographic peaks (Figure S3). Comparison of the quantification results revealed that the latter approach provided slightly more reproductible and accurate results, so this method was chosen. Internal recalibration of both m/z and ion mobilities was performed after each data acquisition. Experimentally measured ion mobility values were converted to CCS values using the fundamental low-field (Mason-Schamp) equation, with T set arbitrarily to 305 K. Ion mobility resolving powers were calculated using the CCS-based definition ($R_p = CCS/\Delta_{fwhm}CCS$)[34].

For the GC-sectorHRMS analysis, data processing was performed using TargetLynx (Waters, version 4.1). The chromatographic area of the two most intense isotopologues of the molecular cluster was used for quantification and confirmation.

3. Results & discussion

3.1 Accumulation time optimization

Since the release of the timsTOF Pro by Bruker, dual-stage ion mobility cells have enabled parallel accumulation and analysis, allowing up to 100% ion utilization[35], which is particularly advantageous for detecting trace compounds. However, increasing accumulation time raises ion density, which can reduce resolving power due to charge repulsion and peak broadening[31,36]. The TIMS cell also has a finite ion capacity and may saturate, making it essential to balance sensitivity (ion count) and selectivity (resolving power)[35].

To optimize accumulation time, a mixture of PBDE congeners (20 pg each) was analyzed across accumulation times from 10 to 250 ms, with analysis time fixed at 250 ms. As expected, signal intensity increased and resolving power decreased with longer accumulation (Figure S4a). Interestingly, some congeners showed linear signal increases, while others plateaued near 100 ms, despite equal injected amounts. This behavior correlated with retention time as later-eluting compounds were more prone to signal saturation (Figure S4b). This trend could be attributed to GC column bleed at higher temperatures, which increases background ion levels, particularly from siloxanes, and can saturate the TIMS cell. Supporting this hypothesis, the experiment was repeated in negative APCI mode, where siloxane ionization was suppressed, reducing background signal by ~100-fold (Figure S5b). Under these conditions, all congeners, including late-eluting ones, exhibited linear signal increases with accumulation time, confirming the impact of background ions on TIMS saturation (Figure S5a). However, due to significantly lower absolute signal in negative mode, it was not used further.

Overall, in positive APCI mode, an accumulation time between 50 and 100 ms seem to provide the best compromise between sensitivity and resolving power. Longer times do not enhance signal intensity due to saturation and space-charge effects. An accumulation time of 75 ms (30% duty cycle) was therefore selected for the PCB fraction. In contrast, for the dioxins fraction, the accumulation time was maintained at 250 ms (i.e., 100% duty cycle). This choice was motivated by the observation that, for analytes present at very low concentrations, signal quality was improved at higher duty cycles. Since dioxins are typically found at ultra-trace levels (ppt to sub-ppt range, compared to ppb to ppt for most PCBs), maximizing the duty cycle ensured more reliable peak integration.

Lastly, the use of ion charge control (ICC) was evaluated. While ICC can prevent overload by adjusting accumulation time, it proved counterproductive here. During high-temperature phases, strong background signals triggered ICC to reduce accumulation below 20 ms, significantly lowering sensitivity for late-eluting analytes (Figure S6). Consequently, ICC was not applied in this study.

3.2 Quantitative performances evaluation of GC-APCI-TIMS-TOF

The assessment of the quantitative performances of our method was performed according to protocols and criteria from the European Regulation 2017/644[37], which states the basic requirements that need to be met by analytical method for the confirmatory analysis of dioxins and PCBs in food. The following criteria were evaluated in this study: linearity, LOQ, precision, trueness and measurement uncertainty. They are discussed in the following subsections. For comparison purposes, the precision, trueness and uncertainty were also determined on our validated GC-EI-sectorHRMS instrument.

3.2.1 Linearity and LOQs

Linearity is commonly evaluated using the coefficient of determination (R^2). However, in the field of dioxin and PCB analysis, where isotope dilution is the reference quantification approach, a more statistically robust method involves assessing linearity through the precision (expressed as RSD) of the relative response factor (RRF), calculated at each calibration level. To determine the linear dynamic range of our method, calibration solutions were analyzed in triplicate over three separate days. For each level, the mean RRF was calculated, and the RSD (%) of these average RRFs was determined. In accordance with regulatory requirements, the RSD must remain below 20% to confirm acceptable linearity. The linear ranges that met this criterion are summarized in Table 1 for each analyte, along with the corresponding RSD values of the average RRF_{avg}. For most PCDDs and PCDFs, the lowest calibration level fell outside the linear range and was excluded. Similarly, for MO and NDL PCBs, the first two calibration points had to be removed to achieve an RSD below 20% (Table S1).

Table 1: Linearity and LOQs obtained with the GC-APCI-TIMS-TOFMS instrumentation for the different analytes.

Analyte	RSD RRF_{avg} (%)	Linear range (pg/μL)	RSD lowest calibration point (n=3, %)	Deviation lowest calibration point compared to RRF_{avg} (%)	iLOQ (pg/μL)	mLOQ (pg/g)	
						2g	4g
2,3,7,8-TCDD	4.9	0.1-10	5.3	-1.2	0.1	0.1	0.05
1,2,3,7,8-PeCDD	4.4	0.1-10	12.4	+7.1	0.1	0.1	0.05
1,2,3,4,7,8-HxCDD	4.4	0.2-20	4.7	-2.1	0.2	0.2	0.1
1,2,3,6,7,8-HxCDD	5.3	0.2-20	12.7	-1.0	0.2	0.2	0.1
1,2,3,7,8,9-HxCDD	4.2	0.2-20	5.2	-2.9	0.2	0.2	0.1
1,2,3,4,6,7,8-HpCDD	4.8	0.2-20	14.2	+6.7	0.2	0.2	0.1
OCDD	5.0	0.5-50	8.1	-1.8	0.5	0.5	0.25
2,3,7,8-TCDF	3.0	0.1-10	9.9	+3.9	0.1	0.1	0.05
1,2,3,7,8-PeCDF	4.1	0.1-10	4.1	+1.6	0.1	0.1	0.05
2,3,4,7,8-PeCDF	3.7	0.1-10	3.8	-3.1	0.1	0.1	0.05
1,2,3,4,7,8-HxCDF	3.6	0.2-20	9.8	+5.0	0.2	0.2	0.1
1,2,3,6,7,8-HxCDF	2.7	0.2-20	1.8	+1.0	0.2	0.2	0.1
2,3,4,6,7,8-HxCDF	4.0	0.2-20	4.0	-5.9	0.2	0.2	0.1
1,2,3,7,8,9-HxCDF	2.8	0.2-20	2.8	-0.3	0.2	0.2	0.1
1,2,3,4,6,7,8-HpCDF	4.1	0.2-20	4.1	-1.3	0.2	0.2	0.1
1,2,3,4,7,8,9-HpCDF	4.9	0.2-20	14.3	+3.3	0.2	0.2	0.1
OCDF	4.0	0.5-50	4.0	-2.7	0.5	0.5	0.25
TCB 81	6.3	0.5-20	0.7	+3.7	0.5	2.7	1.35
TCB 77	5.4	0.5-20	1.8	+5.6	0.5	13.1	6.5
PeCB 126	2.0	0.5-20	4.7	-0.7	0.5	0.5	0.25
HxCB 169	5.5	0.5-20	11.0	+1.0	0.5	0.5	0.25
PeCB 123	2.5	4-140	1.2	-1.1	4	5.7	2.85
PeCB 118	6.5	4-140	10.1	+12.7	4	144	72
PeCB 114	1.5	4-140	4.9	+1.1	4	4.8	2.4
PeCB 105	2.5	4-140	9.0	+2.9	4	53.5	26.75
HxCB 167	3.5	4-140	2.8	-2.7	4	4	2
HxCB 156	5.6	4-140	5.6	-1.1	4	4.0	2.0

HxCB 157	2.0	4-140	3.9	-1.4	4	4	2
HpCB 189	3.1	4-140	4.6	+0.8	4	4	2
TriCB 28	7.8	4-500	4.5	+12.9	4	1299	649.5
TCB 52	9.6	4-500	4.5	+18.4	4	2379	1189.5
PeCB 101	3.0	4-500	1.4	+3.7	4	636	318
HxCB 153	4.2	4-500	5.8	-2.5	4	121	60.5
HxCB 138	3.2	4-500	4.3	-2.3	4	68	34
HpCB 180	4.7	4-500	4.0	-4.9	4	15	7.5

Concerning the limit of quantification (LOQ), two types were determined in this work: the instrumental LOQ (iLOQ) which depends purely on the instrumental performances and the method LOQ (mLOQ) which takes into account the blank levels[27]. The determination of the iLOQ was based on the definition of the LOQ in the regulation[37], where it is stated that it corresponds to "the concentration of an analyte in the extract of a sample which produces an instrumental response at two different ions to be monitored with a S/N (signal/noise) ratio of 3:1 for the less intensive raw data signal". Moreover, the regulation specifies that "if for technical reasons the signal-to-noise calculation does not provide reliable results" the LOQ can be defined as "the lowest concentration point on a calibration curve that gives an acceptable (≤ 30 %) and consistent (measured at least at the start and at the end of an analytical series of samples) deviation to the average relative response factor calculated for all points on the calibration curve in each series of samples". While the S/N-based definition is commonly used with traditional GC-sectorHRMS methods, we found it unsuitable for the GC-TIMS-TOF system. The additional ion mobility separation effectively acts as a noise filter, suppressing background signals to such an extent that calculating a representative noise level—and consequently, a reliable signal-to-noise ratio—is no longer feasible (Figure S7). A similar limitation has already been reported for GC-QqQ systems[27]. Therefore, the iLOQ in this work was determined according to the second regulatory definition. Specifically, it was set as the lowest calibration point for which the average RRF, measured over three different days, met two criteria: (i) a relative standard deviation (RSD) ≤ 15%, and (ii) a deviation of less than 30% from the overall average RRF across the entire calibration range.

The resulting iLOQs are displayed in Table 1. For all analytes, the lowest calibration point within the linear range satisfied both criteria and was thus designated as the iLOQ. These results demonstrate that the GC-APCI-TIMS-TOF platform offers sufficient intrinsic sensitivity to quantify analytes at sub-ppt levels, with absolute concentrations in the range few hundreds of femtograms per μL, i.e. concentrations typically encountered in injection vials after sample preparation of food samples.

As regards to the mLOQ, it was calculated as the mean contamination levels in 10 procedural blanks plus ten times standards deviations. Procedural blanks were prepared weekly to reflect routine laboratory conditions. For the NO PCB 169 and all the PCDD/Fs which were not found in the procedural blanks, the mLOQ was set equal to the corresponding iLOQ. The conversion from iLOQ to mLOQ assumed a final extract volume of 10 µL, an injection volume of 5 µL, and 100% recovery. For a few compounds detected in the blanks, specifically PeCB 126, HxCB 167, HxCB 157, and HpCB 189, the calculated mLOQ based on contamination levels was lower than the value derived from the iLOQ. In these cases, the higher of the two values was retained to ensure conservativeness. The resulting mLOQs are reported in Table 1, based on sample masses of 2 g (fish oil) and 4 g (palm oil and milk fat).

Overall, the mLOQs were in the high fg/g for the dioxins and ranged from a few pg to hundreds of pg/g for the dioxin like PCBs. The mLOQs for the NDL PCBs were much higher owing to their relatively high level in the procedural blanks, in particular for the PCBs 28, 52 and 101. It is important to emphasize that, for most PCB congeners, the mLOQs reported in Table 1 do not reflect the sensitivity of the TIMS-TOF Pro2 instrument itself, but rather the background contamination observed in our laboratory environment, which severely penalizes the achievable LOQs for these congeners.

3.2.2 Precision, trueness and uncertainty

The precision, trueness, and uncertainty of the method were evaluated using a set of samples from proficiency tests for which consensus concentration values of the target congeners were available. Six aliquots of each matrix (palm oil, fish oil, and milk fat) were analyzed over five days under intermediate reproducibility conditions using the GC-TIMS-TOF method. For comparison, an additional set of six aliquots per matrix was prepared and analyzed under the same conditions using our reference GC-sectorHRMS instrument.

Intermediate precision (RSD_R) was estimated for each congener by calculating the relative standard deviation across the six replicate measurements. The resulting RSD_R values for both the TIMS and sector methods are plotted as a function of analyte concentration in Figures 1a and 1b, respectively. These plots clearly show that, in the vast majority of cases (97%), the RSD_R values obtained with the TIMS method remained below the regulatory thresholds of 15% for PCDD/Fs and DL PCBs, and 20% for NDL PCBs. Moreover, comparison of Figures 1a and 1b indicates that the precision achieved with the TIMS method was broadly comparable to that of the sector instrument. On average, the RSD_R was slightly higher with the TIMS method for

dioxins (8.9% vs. 6.1%), but slightly lower for the NDL PCBs (5.0% vs. 8.1%) (Table S8). As expected, for both techniques, RSD_R values tended to approach the regulatory thresholds at lower analyte concentrations.

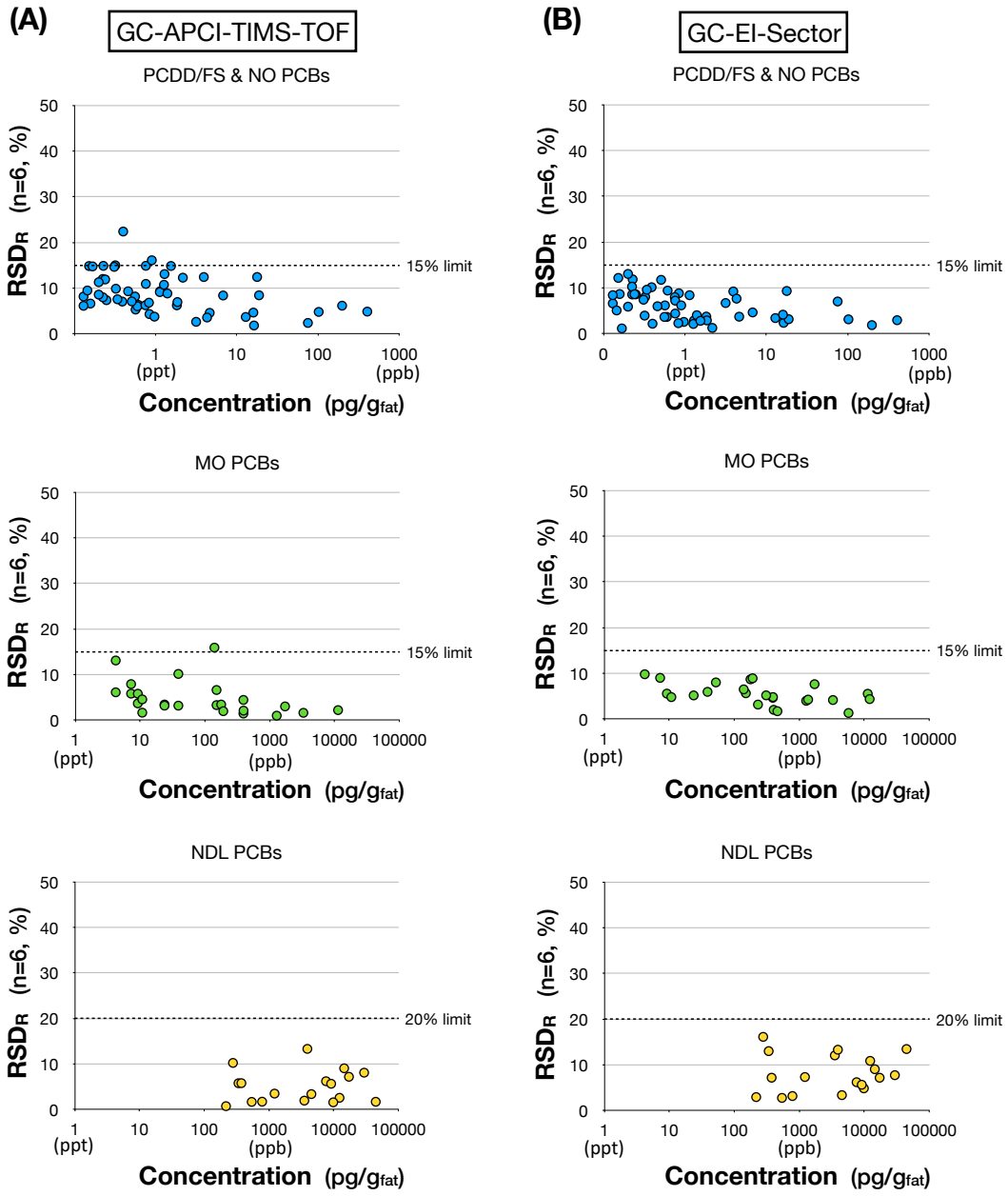

Figure 1: Plot of RSD_R versus concentrations of the analytes in the different samples for (A) the GC-APCI-TIMS-TOFMS and (B) GC-EI-Sector methods.

Trueness was assessed through the calculation of the bias of the measured values with respect to the consensus values from the PTs. The resulting biases for PCDD/Fs, DL PCBs and NDL PCBs are plotted against analyte concentration in Figure 2a (TIMS) and 3b (sector). With regards to the PCDD/Fs fraction, the plot indicates that the calculated biases with the TIMS instrumentation globally complied with the European requirements (79.9% of biases were within the +/- 20% threshold, Table S8). Although a notable portion of biases exceeded this threshold, especially at lower concentrations (around the ppt level and below), this high compliance rate for trueness remains very encouraging, particularly given the complexity of the matrix and the ultra-trace levels of PCDD/Fs involved. This trend contrasts with the performance of the sector instrument, where nearly all biases (99.7%) were within regulatory limits, although a slight increase in variability was observed at the lowest concentration levels. Accordingly, the mean absolute bias for dioxins was almost twice as high with the TIMS system

compared to the sectorHRMS method (13.1% vs. 7.3%, Table S8), suggesting a limitation of the current TIMS configuration in accurately quantifying PCDD/Fs at ultra-trace levels close to the mLOQ.
For the PCBs fraction, biases were generally well within the regulatory acceptance criteria: 87.2% of values fell within ±20% for MO PCBs, and 93.0% within ±30% for NDL PCBs. These results compared favourably with the sectorHRMS method, with mean absolute biases of 8.9% vs. 7.1% for MO PCBs, and 9.8% vs. 10.3% for NDL PCBs (Table S8), confirming the trueness performances of the GC-TIMS-TOF platform for PCB quantification across a broad concentration range.

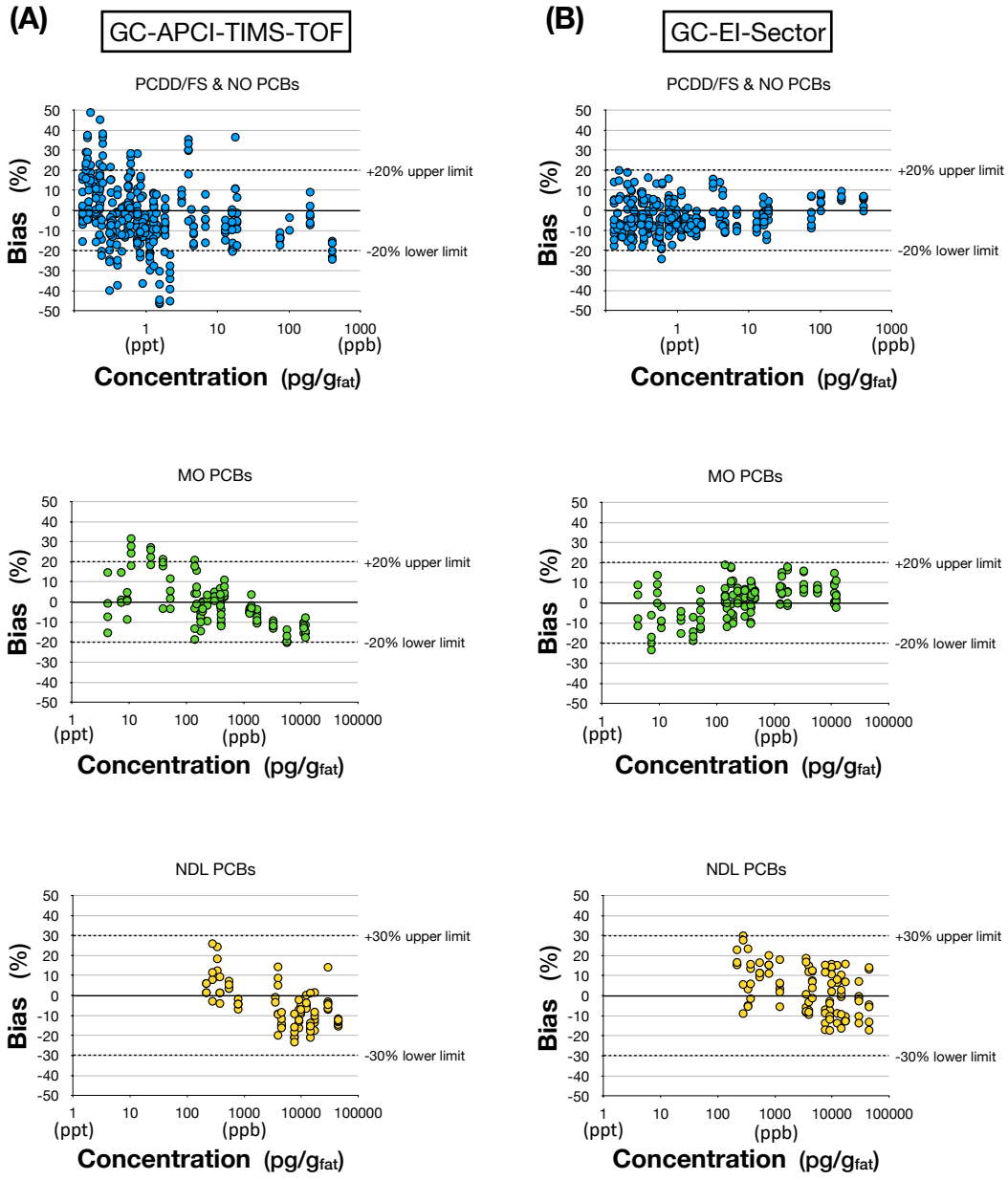

Figure 2: Plot of bias versus concentrations of the analytes in the different samples for (A) the GC-APCI-TIMS-TOFMS and (B) GC-EI-Sector methods.

Measurement uncertainty was estimated using the top-down approach developed by the EURL POPs[38], based on intermediate precision and trueness. As illustrated in the bar graph in Figure S8, the calculated expended uncertainty U (with a coverage factor of 2) for PCDDs and PCDFs with the TIMS method was generally higher than that observed for PCBs. Moreover, for approximately half of the dioxin congeners, the calculated uncertainties were moderately to significantly higher (e.g., 1,2,3,7,8,9-HpCDF, OCDF) than the EURL recommended value[38] (U ≤ 38%). These findings are primarily attributed to a greater contribution of trueness at very low concentrations, which becomes more pronounced for PCDD/Fs in the TIMS method. In contrast, uncertainties for PCBs were generally comparable between the two techniques.

Finally, the precision, trueness and uncertainty were also evaluated for the summed WHO_{2005}-TEQ concentrations of PCDD/FS and DL PCBs, as well as the sum concentrations of NDL PCBs. For each matrix, all performance criteria complied with the regulation requirements (Table S9 and Figure S8) and the total TEQ concentrations measured with both instruments were in close agreement (Figure 3). Importantly, both methods led to the same compliance conclusions for all three samples with respect to their respective PCDD/Fs maximum limits[39], demonstrating the reliability of the TIMS approach compared to the reference sector field instrument at ppt levels . One exception to this consistency was observed for the milk fat sample, where the summed TEQ concentrations of dioxins and DL-PCBs, as well as the summed NDL-PCB concentration, were classified as compliant using the TIMS method, but as non-compliant with the sector instrument, once expanded uncertainties were taken into account (Figure 3 and Table S9). Importantly, TIMS also measured concentrations above the respective maximum levels, consistent with the sector instrument (Figure 3). However, since the measured values were only slightly above the regulatory thresholds, and the expanded uncertainty associated with TIMS was slightly larger, the compliance decision fell within the uncertainty range, resulting in a classification as compliant. In such borderline cases, the alternative approach using TIMS would trigger the need for confirmatory analysis, as required by regulation. This clearly demonstrates that TIMS fulfilled its intended role as a reliable alternative screening method at the maximum level decision, and that, in any case, the appropriate decision had been made for the sum of PCDD/Fs in this milk fat sample limiting the risk of false non-compliance.

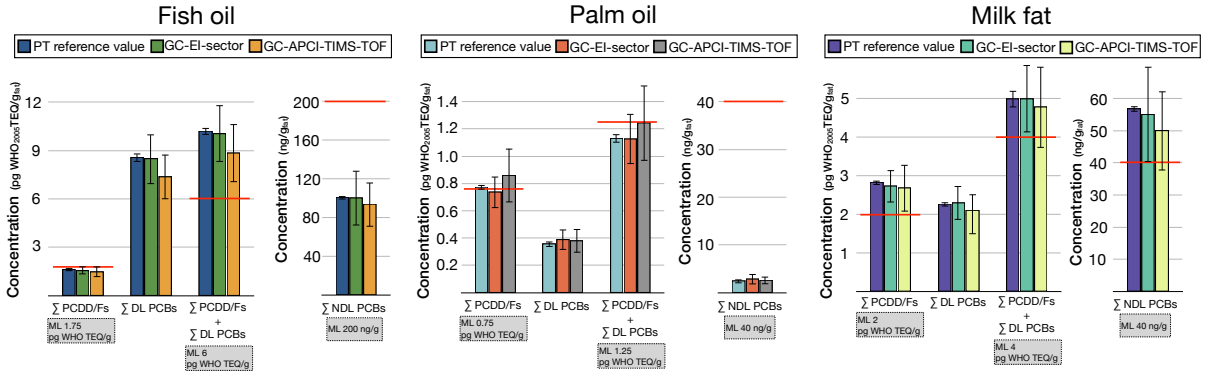

Figure 3: Comparison of total upper bound WHO_{2005} TEQ concentrations of dioxins (PCDDs + PCDFs) and dioxin like PCBs (NO + MO PCBs) and summed concentrations of NDL PCBs measured by GC-EI-sector and GC-APCI-TIMS-TOF in the different matrices. The horizontal red lines correspond to the maximum limits according to commission regulation EU 2023/915*[39]*. The error bars correspond to the expended measurement uncertainties (Figure S8).

3.3 Benefits of ion mobility for the quantitative analysis of contaminants

3.3.1 CCS values for analyte confirmation

The identification of an analyte by targeted GC-MS methods is usually confirmed through retention times comparison between the analyte and its isotopically labelled standard analogue (e.g., <0.15%) as well as compliance of the ion abundance ratios (e.g., +/- 15% around the theoretical value)[37]. The addition of an ion mobility step within this workflow provides an additional means to correctly confirm the identity of the analyte and thus avoid false positives. In screening and non-targeted approaches, comparison between experimental CCS and references values from libraries (built in-house or made available from other laboratories) has already shown great promises to improve confidence in analyte assignment. Indeed, it was demonstrated that CCS values are not affected by the sample matrix[40,41] and generally display good reproducibility across different instrumental designs[42–44]. As a result, a 2% variation between experimental and reference database value has been suggested several times in the literature as a plausible cut-off value for identity confirmation of the analytes[40,45,46].

In targeted analysis performed with the isotopic dilution method, the CCS values can directly be compared between the analyte and its isotopically labelled standard, since both are present simultaneously in a given sample. In this work, we found the CCS of the native and corresponding labelled standard to be really close. On average, the CCS difference between native and standard at the different calibration levels varied from a minimum of 0.00% to a maximum of 0.21% (Figure S9). The differences were greatest for lower chlorinated PCBs, especially those with three and four chlorine atoms (Figure 4a) but decreased with increasing halogenation degree. Moreover, they were not significant for the PCDDs and the PCDFs (Figure 4b). It is noteworthy that, when present, the differences in CCS were consistently attributable to the isotopically labelled standard exhibiting a slightly higher CCS in comparison to the native analyte (Figures 4a and S10). This systematic behaviour is akin to the relative differences in the GC retention times where the ^{13}C labelled standards always elute a few seconds

before their native analogues. The reason for these small deviations in CCS could be due to isotopic effects (i.e., isotopologue effect[47]).

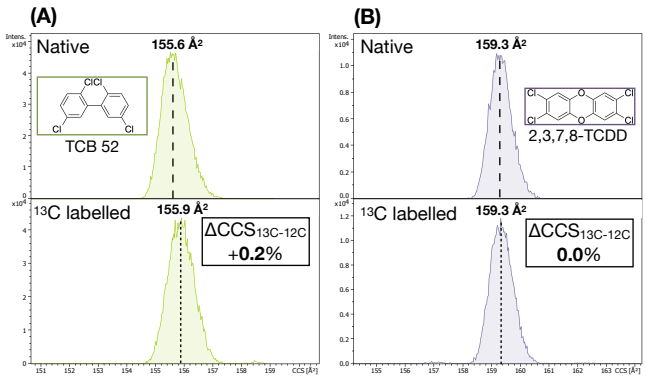

Figure 4: Overlayed ion mobility spectra of the native and ^{13}C labelled standards of (A) TCB 52 and (B) 2,3,7,8-TCDD (calibration level 5 in each case). A slight difference in CCS between the two standards can be seen in the case of the TCB 52.

In addition, a gradual CCS shift towards higher values was observed for the PCBs starting at the calibration level 7 (corresponding to an injection of 80 pg of native + 20 pg of labelled standard, Figure S9). These shifts are likely the result of space charge effects arising from increased ion density at the trapping region within the TIMS tunnel. However, since these CCS shifts affected both the native analytes and their isotopically labelled analogues, the relative CCS differences between them were generally preserved. Only minor increases in ΔCCS were observed for a few analytes, with the largest shift reaching 0.45% for TCB 52 (Figure S10).

In light of these findings, we propose that a conservative cut-off of 0.5% for the maximum allowable CCS difference between an analyte and its labelled internal standard could serve as an additional identity confirmation criterion when using isotope dilution for quantification. This approach would add an extra level of selectivity, further enhancing the confidence in compound identification within the TIMS-based workflow.

3.3.2 Increased selectivity

The additional dimension of separation provided by ion mobility has been shown on numerous occasions to allow for the separation of isomers and isobars[41,48]. In addition to providing cleaner mass spectra that can aid in the identification of features in suspect and non targeted workflows[49] (e.g., comparison of an experimental tandem spectrum with a reference), removing isomeric and isobaric interferences is important to avoid overestimating the concentrations and therefore obtain accurate quantification of the analytes.

In this work, most of the 35 target analytes were not impacted by potential interferences. This is due to a combination of a very thorough sample preparation which destroys and removes the great majority of the matrix and a high resolution separation in both the chromatographic and the mass spectrometric dimension (R_{FWHM} > 40 000). However, a number of interferences were still observed in some matrices. These were, for the great majority, partial coelution of isomeric congeners. For instance in the palm oil sample, numerous TCDDs were present in the sample and one of them was partially coeluting with the 2,3,7,8-TCDD (Figure 5a). However, in the IM dimension, the 2,3,7,8-TCDD was baseline separated from this interference (Figure 5c) and this interference could be removed in the corresponding IM-filtered chromatogram (Figure 5b). Similar cases were also observed for the NDL-PCBs 52, 101 and 153 in the different matrices (Figure S11). In the case of the TriCB 28, while a single peak was observed in the chromatographic dimension, the corresponding ion mobility spectrum strongly suggested the presence of an interfering compound (Figure S12). Here only a partial separation could be obtained. The TriCB 31 is a well known coeluting interference of TriCB 28. This coelution was resolved with the sector instrumentation by using a specific GC column (HT-8). For the TIMS configuration, a classic and more versatile column was used (DB5-MS).

With the exceptions of the few cases discussed in the previous paragraph, overall most of the partially coeluting isomers observed in the different samples could not be further separated in the IM dimension, despite the high resolving power of the method (Figure S13). This observation is consistent with the results in another study[46] and in our previous work, where we found that the separation of (partially) coeluting polyhalogenated pollutant isomers was usually not achieved in the IM dimension even at very high resolving power (Rp ~200)[33].

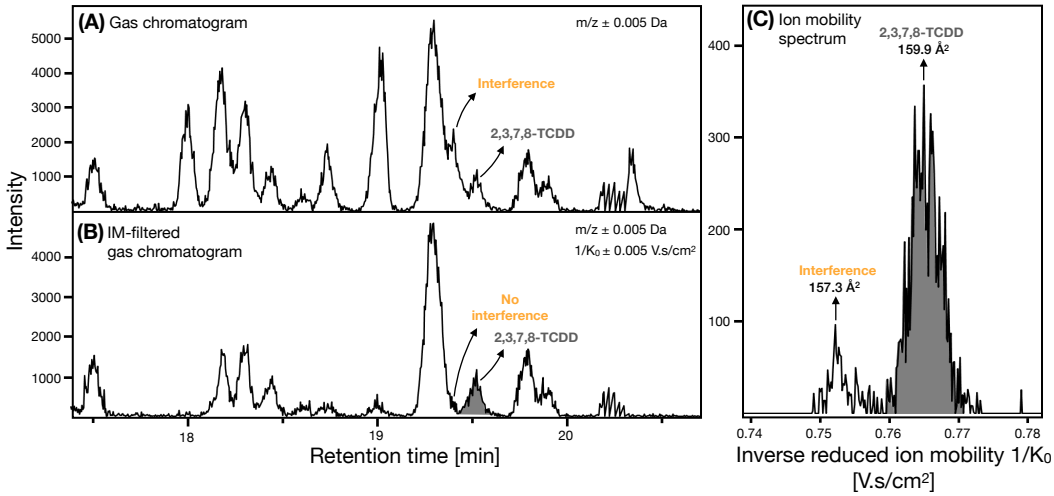

Figure 5: Unfiltered (A) and IM-filtered (B) gas chromatograms of 2,3,7,8-TCDD in the palm oil sample. (C) Corresponding ion mobility spectrum of 2,3,7,8-TCDD.

Besides coeluting isomers, another type of interference that was observed was the case of two coeluting isobars, the 1,2,3,7,8-PeCDD and the HxCB 169 (Figure S14). Here, the M+6 isotopologue of the PeCDD (m/z 359.8485) interferes with the most intense isotopologue of the HxCB used for quantification (M+2, m/z 359.8410). The same isobaric interference is observed between the corresponding isotopically labelled standards (m/z 371.8885 vs m/z 371.8812). However, these interferences were completely resolved in the ion mobility dimension, the CCS of the hexachloro substituted PCB being significantly larger than that of the pentachloro substituted PCDD (Figure S14).

Finally, a last type of interference was noticed in the case of the MO-PCB 123 (Figure 6). This PeCB was partially coeluting with two other PCB congeners, a PeCB and an HxCB (Figure 6a). The difference in CCS between the two PeCBs was too small to obtain an appreciable separation, leaving the interfering PeCB appear as a small shoulder on the right of the ion mobility peak of PCB 123 (Figure 6b). Concerning the HxCB, this type of coelution is not, a priori, an issue, since in positive APCI, the soft ionization mechanism gives mostly rise to intense parent ions (~85% $[M]^{+\cdot}$ and ~15% $[M+H]^{+}$) that can be readily distinguished in the m/z dimension (i.e., m/z 325.8799 for PeCBs and m/z 359.8410 for HxCBs). Nevertheless, we observed that a small extent of fragmentation (1 to 2%) still generally occurred for PCBs in the form of $[M+H-Cl]^{+\cdot}$ and $[M-Cl]^{+\cdot}$ ions. These types of fragments can turn out problematic in the event of a coelution between two PCB congeners that differ by one degree of chlorination, especially if the most chlorinated congener is much more present in the sample compared to the other. Indeed, in this situation these fragments become isomeric/isobaric interferences with regard to the less chlorinated PCB. This was typically the case here with the PeCB 123 and the coeluting HxCB congener which had a signal intensity more than an order of magnitude higher.

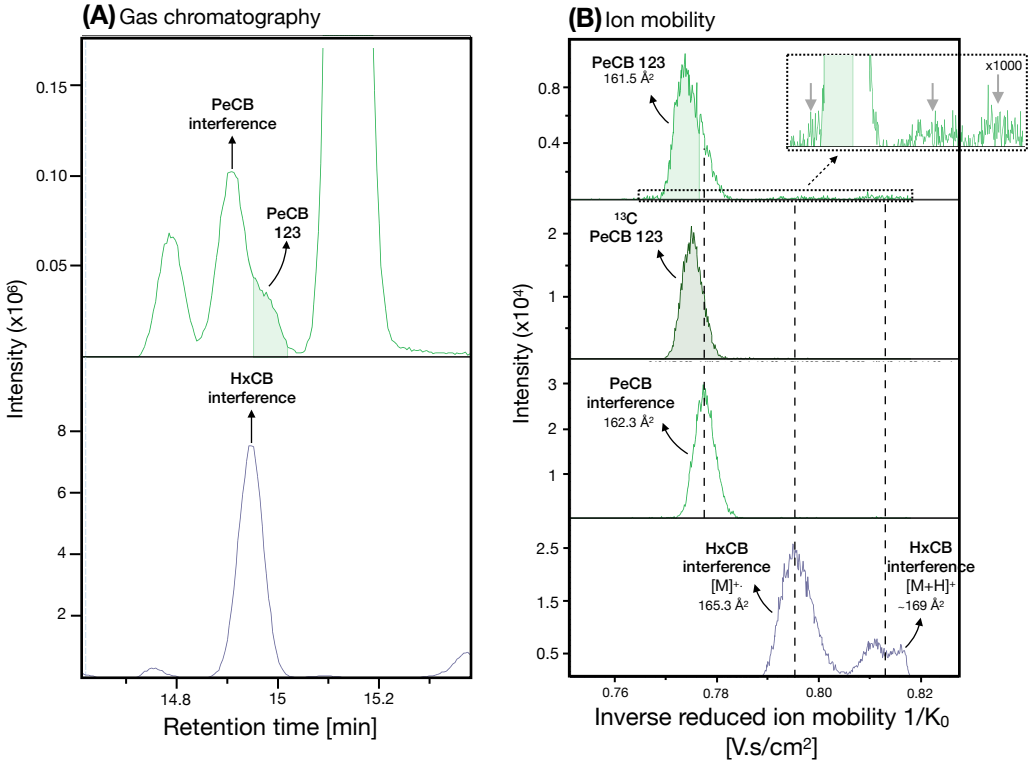

Figure 6: (A) Overlaid chromatograms of PeCBs and HxCBs close to the retention time of PeCB 123 (milk fat sample). (B) Overlaid ion mobility spectra of PeCB 123, its ^{13}C standard analog, the coeluting PeCB interference and the coeluting HxCB interference. For the HxCB interreference, the IM peaks from both types of parents ions ($[M]^{+\cdot}$ and $[M+H]^+$) are shown in the spectrum since both can give rise to isomeric/isobaric fragments.

However, the additional ion mobility dimension can, at least partially, resolve this issue. Indeed, depending on the moment the fragmentation takes relative to the ion mobility separation, some separation can be achieved between the analyte and the interfering fragment ions[50] (Figure S15). In the case of fragmentations taking place before or during the separation (e.g., in source, in transit to the IM cell, etc.), the fragment ions go through the TIMS cell, become trapped and elute at a later time compared to their precursor ions since they are characterized by lower CCS values (in TIMS, ions with the highest CCS elute first, Figure S15a). Moreover, since these fragments are isomeric/isobaric to the analyte ion, the probability that they share a similar CCS is high. Therefore in this case, IM separation of the analyte ion and the fragment ions is not likely. However, in the case of fragmentations occurring after the IM separation (in transit to the TOF MS), the ion mobility of the fragments match that of their precursor ions (Figure S15b). This time, the separation between the analyte ion and the isomeric/isobaric fragment ions is much more likely since two PCBs congeners differing by one chlorine atom are usually characterized by CCS that are sufficiently different to obtain a baseline separation at the resolving power of the TIMS (see Section 3.1.1).

This is indeed what is observed in Figure 6b. In the mobility spectrum of the PeCB 123 $[M]^{+\cdot}$ ion, a series of peaks of small intensity can be seen on the right side of the major peak at higher CCS values (see inset in Figure 6b). These are the signal corresponding to the post IM fragmentation of the coeluting HxCB interference. This is confirmed by the alignment of those signals with the ion mobility peaks of their precursor $[M]^{+\cdot}$ and $[M+H]^+$ ions (bottom ion mobility spectrum in Figure 6b). As for the series of low intensity peaks on the left side of the major peak (see inset), they could be attributed to signal originating from the pre/intra IM fragmentation of the coeluting HxCB. Some of this signal may not be visible due to overlap with that of the PeCB 123 $[M]^{+\cdot}$ ion.

Clearly, in this example, the impact of the HxCB isomeric fragment ions is negligible due to the low relative intensity of their signal. However, such types of interference could become significantly more pronounced in samples where the intensity difference between the interfering fragment and the target analyte is smaller, or in the case of compound classes that exhibit a higher degree of fragmentation under positive APCI conditions (e.g., PCDDs, as illustrated in Figure S16). In such scenarios, the additional selectivity offered by the ion mobility dimension could prove particularly beneficial, enabling the separation of interfering species and thus improving the accuracy and reliability of the quantification.

4. Conclusions

In this work, the potential of a modern IM-MS platform, namely a TIMS-TOF instrument, to perform quantitative analysis of trace and ultra-trace contaminants was assessed. The performance evaluation conducted demonstrated that the GC-APCI-TIMS-TOF method we developed broadly met the requirements of EU Regulation 2017/644 in terms of linearity, LOQs, precision, trueness, and measurement uncertainty for PCDD/Fs and PCBs in three different fat and oil samples. Although a non-negligible fraction of individual PCDD/F congeners—present at very low levels (around ppt and below)—showed accuracies falling outside the tolerated range, this had only a limited impact on the overall method performance: all regulatory criteria were fulfilled for the summed TEQ concentrations, which are the key metrics for regulatory compliance. Compared to the reference GC-sector HRMS method, performances were similar or slightly lower for PCBs, and slightly to significantly lower for most PCDD/Fs. However, the added ion mobility separation dimension of the GC-APCI-TIMS-TOF method brought significant advantages in terms of analyte identification (with CCS values serving as an additional identification point in targeted analysis) and peak capacity (enabling separation of some partially coeluting isomers, isobars, and isomeric fragment ions). This improved selectivity for dioxins and PCBs could potentially allow for simplified sample preparation procedures. Furthermore, the full-scan acquisition mode of the TOF instrument allows for simultaneous screening of unknown compounds, in contrast to the SIM mode of sector MS, which limits detection to a predefined set of target analytes. Additionally, the method enables the monitoring of multiple contaminant classes within a single run, offering potential savings in both analysis time and cost[51].Overall, this study highlights the promising potential of the TIMS-TOF platform and IM-MS technologies more generally for the quantitative analysis of a broad range of contaminants in complex matrices.

References

(1) Gabelica, V. CHAPTER 1. Ion Mobility–Mass Spectrometry: An Overview. In *New Developments in Mass Spectrometry*; Ashcroft, A. E., Sobott, F., Eds.; Royal Society of Chemistry: Cambridge, 2021; pp 1–25. https://doi.org/10.1039/9781839162886-00001.

(2) Eiceman, G. A.; Karpas, Z.; Hill, H. H. *Ion Mobility Spectrometry*, Third edition (Online-Ausg.).; Taylor & Francis: Boca Raton, 2014.

(3) Ewing, R. A Critical Review of Ion Mobility Spectrometry for the Detection of Explosives and Explosive Related Compounds. *Talanta* **2001**, *54* (3), 515–529. https://doi.org/10.1016/S0039-9140(00)00565-8.

(4) Armenta, S.; Garrigues, S.; De La Guardia, M.; Brassier, J.; Alcalà, M.; Blanco, M.; Perez-Alfonso, C.; Galipienso, N. Detection and Characterization of Emerging Psychoactive Substances by Ion Mobility Spectrometry. *Drug Test. Anal.* **2015**, *7* (4), 280–289. https://doi.org/10.1002/dta.1678.

(5) Mäkinen, M. A.; Anttalainen, O. A.; Sillanpää, M. E. T. Ion Mobility Spectrometry and Its Applications in Detection of Chemical Warfare Agents. *Anal. Chem.* **2010**, *82* (23), 9594–9600. https://doi.org/10.1021/ac100931n.

(6) Zheng, X.; Wojcik, R.; Zhang, X.; Ibrahim, Y. M.; Burnum-Johnson, K. E.; Orton, D. J.; Monroe, M. E.; Moore, R. J.; Smith, R. D.; Baker, E. S. Coupling Front-End Separations, Ion Mobility Spectrometry, and Mass Spectrometry For Enhanced Multidimensional Biological and Environmental Analyses. *Annu. Rev. Anal. Chem.* **2017**, *10* (1), 71–92. https://doi.org/10.1146/annurev-anchem-061516-045212.

(7) Kanu, A. B.; Hill, H. H. Ion Mobility Spectrometry Detection for Gas Chromatography. *J. Chromatogr. A* **2008**, *1177* (1), 12–27. https://doi.org/10.1016/j.chroma.2007.10.110.

(8) Kanu, A. B.; Dwivedi, P.; Tam, M.; Matz, L.; Hill, H. H. Ion Mobility–Mass Spectrometry. *J. Mass Spectrom.* **2008**, *43* (1), 1–22. https://doi.org/10.1002/jms.1383.

(9) Celma, A.; Alygizakis, N.; Belova, L.; Bijlsma, L.; Fabregat-Safont, D.; Menger, F.; Gil-Solsona, R. Ion Mobility Separation Coupled to High-Resolution Mass Spectrometry in Environmental Analysis – Current State and Future Potential. *Trends Environ. Anal. Chem.* **2024**, *43*, e00239. https://doi.org/10.1016/j.teac.2024.e00239.

(10) Song, X.-C.; Canellas, E.; Dreolin, N.; Goshawk, J.; Lv, M.; Qu, G.; Nerin, C.; Jiang, G. Application of Ion Mobility Spectrometry and the Derived Collision Cross Section in the Analysis of Environmental Organic Micropollutants. *Environ. Sci. Technol.* **2023**, *57* (51), 21485–21502. https://doi.org/10.1021/acs.est.3c03686.

(11) Barnett, D. A.; Guevremont, R.; Purves, R. W. Determination of Parts-per-Trillion Levels of Chlorate, Bromate, and Iodate by Electrospray Ionization/High-Field Asymmetric Waveform Ion Mobility Spectrometry/Mass Spectrometry. *Appl. Spectrosc.* **1999**, *53* (11), 1367–1374. https://doi.org/10.1366/0003702991945984.

(12) Ells, B.; Barnett, D. A.; Purves, R. W.; Guevremont, R. Trace Level Determination of Perchlorate in Water Matrices and Human Urine Using ESI-FAIMS-MS. *J. Environ. Monit.* **2000**, *2* (5), 393–397. https://doi.org/10.1039/b005601o.

(13) Handy, R.; Barnett, D. A.; Purves, R. W.; Horlick, G.; Guevremont, R. Determination of Nanomolar Levels of Perchlorate in Water by ESI-FAIMS-MS. *J. Anal. At. Spectrom.* **2000**, *15* (8), 907–911. https://doi.org/10.1039/b002306j.

(14) Gonzalez De Vega, R.; Cameron, A.; Clases, D.; Dodgen, T. M.; Doble, P. A.; Bishop, D. P. "Simultaneous Targeted and Non-Targeted Analysis of per- and Polyfluoroalkyl Substances in Environmental Samples by Liquid Chromatography-Ion Mobility-Quadrupole Time of Flight-Mass Spectrometry and Mass Defect Analysis." *J. Chromatogr. A* **2021**, *1653*, 462423. https://doi.org/10.1016/j.chroma.2021.462423.

(15) Hinnenkamp, V.; Balsaa, P.; Schmidt, T. C. Quantitative Screening and Prioritization Based on UPLC-IM-Q-TOF-MS as an Alternative Water Sample Monitoring Strategy. *Anal. Bioanal. Chem.* **2019**, *411* (23), 6101–6110. https://doi.org/10.1007/s00216-019-01994-w.

(16) Adams, K. J.; Smith, N. F.; Ramirez, C. E.; Fernandez-Lima, F. Discovery and Targeted Monitoring of Polychlorinated Biphenyl Metabolites in Blood Plasma Using LC-TIMS-TOF MS. *Int. J. Mass Spectrom.* **2018**, *427*, 133–140. https://doi.org/10.1016/j.ijms.2017.11.009.

(17) Yan, M.; Zhang, N.; Li, X.; Xu, J.; Lei, H.; Ma, Q. Integrating Post-Ionization Separation via Differential Mobility Spectrometry into Direct Analysis in Real Time Mass Spectrometry for Toy Safety Screening. *Anal. Chem.* **2024**, *96* (1), 265–271. https://doi.org/10.1021/acs.analchem.3c03915.

(18) Shi, Y.; Jin, H.-F.; Shi, M.-Z.; Cao, J.; Ye, L.-H. Carbon Black-Assisted Miniaturized Solid-Phase Extraction of Carbamate Residues from Ginger by Supercritical Fluid Chromatography Combined with Ion Mobility Quadrupole Time-of-Flight Mass Spectrometry. *Microchem. J.* **2023**, *194*, 109335. https://doi.org/10.1016/j.microc.2023.109335.

(19) Shi, Y.; Jin, H.-F.; Ma, X.-R.; Cao, J. Highly Sensitive Determination of Multiple Pesticide Residues in Foods by Supercritical Fluid Chromatography Coupled with Ion Mobility Quadrupole Time-of-Flight Mass Spectrometry. *Food Res. Int.* **2024**, *175*, 113769. https://doi.org/10.1016/j.foodres.2023.113769.

(20) Ray, J. A.; Kushnir, M. M.; Yost, R. A.; Rockwood, A. L.; Wayne Meikle, A. Performance Enhancement in the Measurement of 5 Endogenous Steroids by LC–MS/MS Combined with Differential Ion Mobility Spectrometry. *Clin. Chim. Acta* **2015**, *438*, 330–336. https://doi.org/10.1016/j.cca.2014.07.036.

(21) Moehnke, K.; Kemp, J.; Campbell, M. R.; Singh, R. J.; Tebo, A. E.; Maus, A. Using Differential Mobility Spectrometry to Improve the Specificity of Targeted Measurements of 2,3-Dinor 11β-Prostaglandin F2α. *Clin. Biochem.* **2024**, *126*, 110745. https://doi.org/10.1016/j.clinbiochem.2024.110745.

(22) Lerner, R.; Baker, D.; Schwitter, C.; Neuhaus, S.; Hauptmann, T.; Post, J. M.; Kramer, S.; Bindila, L. Four-Dimensional Trapped Ion Mobility Spectrometry Lipidomics for High Throughput Clinical Profiling of Human Blood Samples. *Nat. Commun.* **2023**, *14* (1), 937. https://doi.org/10.1038/s41467-023-36520-1.
(23) Fan, R.-J.; Zhang, F.; Chen, X.-P.; Qi, W.-S.; Guan, Q.; Sun, T.-Q.; Guo, Y.-L. High-Throughput Screening and Quantitation of Guanidino and Ureido Compounds Using Liquid Chromatography-Drift Tube Ion Mobility Spectrometry-Mass Spectrometry. *Anal. Chim. Acta* **2017**, *961*, 82–90. https://doi.org/10.1016/j.aca.2017.01.036.
(24) Chai, Y.; Grebe, S. K. G.; Maus, A. Improving LC-MS/MS Measurements of Steroids with Differential Mobility Spectrometry. *J. Mass Spectrom. Adv. Clin. Lab* **2023**, *30*, 30–37. https://doi.org/10.1016/j.jmsacl.2023.10.001.
(25) Oranzi, N. R.; Lei, J.; Kemperman, R. H. J.; Chouinard, C. D.; Holmquist, B.; Garrett, T. J.; Yost, R. A. Rapid Quantitation of 25-Hydroxyvitamin D2 and D3 in Human Serum Using Liquid Chromatography/Drift Tube Ion Mobility-Mass Spectrometry. *Anal. Chem.* **2019**, *91* (21), 13555–13561. https://doi.org/10.1021/acs.analchem.9b02683.
(26) Lay, J. O.; Liyanage, R.; Gidden, J. A. THE DEVELOPMENT OF A HIGH-RESOLUTION MASS SPECTROMETRY METHOD FOR ULTRA-TRACE ANALYSIS OF CHLORINATED DIOXINS IN ENVIRONMENTAL AND BIOLOGICAL SAMPLES INCLUDING VIET NAM ERA VETERANS. *Mass Spectrom. Rev.* **2021**, *40* (3), 236–254. https://doi.org/10.1002/mas.21639.
(27) L'Homme, B.; Scholl, G.; Eppe, G.; Focant, J.-F. Validation of a Gas Chromatography–Triple Quadrupole Mass Spectrometry Method for Confirmatory Analysis of Dioxins and Dioxin-like Polychlorobiphenyls in Feed Following New EU Regulation 709/2014. *J. Chromatogr. A* **2015**, *1376*, 149–158. https://doi.org/10.1016/j.chroma.2014.12.013.
(28) Ten Dam, G.; Pussente, I. C.; Scholl, G.; Eppe, G.; Schaechtele, A.; Van Leeuwen, S. The Performance of Atmospheric Pressure Gas Chromatography–Tandem Mass Spectrometry Compared to Gas Chromatography–High Resolution Mass Spectrometry for the Analysis of Polychlorinated Dioxins and Polychlorinated Biphenyls in Food and Feed Samples. *J. Chromatogr. A* **2016**, *1477*, 76–90. https://doi.org/10.1016/j.chroma.2016.11.035.
(29) Focant, J.-F.; Pirard, C.; Eppe, G.; De Pauw, E. Recent Advances in Mass Spectrometric Measurement of Dioxins. *J. Chromatogr. A* **2005**, *1067* (1–2), 265–275. https://doi.org/10.1016/j.chroma.2004.10.095.
(30) Focant, J.-F.; Eppe, G.; Scippo, M.-L.; Massart, A.-C.; Pirard, C.; Maghuin-Rogister, G.; Pauw, E. D. Comprehensive Two-Dimensional Gas Chromatography with Isotope Dilution Time-of-Flight Mass Spectrometry for the Measurement of Dioxins and Polychlorinated Biphenyls in Foodstuffs. *J. Chromatogr. A* **2005**, *1086* (1–2), 45–60. https://doi.org/10.1016/j.chroma.2005.05.090.
(31) Michelmann, K.; Silveira, J. A.; Ridgeway, M. E.; Park, M. A. Fundamentals of Trapped Ion Mobility Spectrometry. *J. Am. Soc. Mass Spectrom.* **2015**, *26* (1), 14–24. https://doi.org/10.1007/s13361-014-0999-4.
(32) Silveira, J. A.; Michelmann, K.; Ridgeway, M. E.; Park, M. A. Fundamentals of Trapped Ion Mobility Spectrometry Part II: Fluid Dynamics. *J. Am. Soc. Mass Spectrom.* **2016**, *27* (4), 585–595. https://doi.org/10.1007/s13361-015-1310-z.
(33) Muller, H. B.; Scholl, G.; Far, J.; De Pauw, E.; Eppe, G. Sliding Windows in Ion Mobility (SWIM): A New Approach to Increase the Resolving Power in Trapped Ion Mobility-Mass Spectrometry Hyphenated with Chromatography. *Anal. Chem.* **2023**, *95* (48), 17586–17594. https://doi.org/10.1021/acs.analchem.3c03039.
(34) Dodds, J. N.; May, J. C.; McLean, J. A. Correlating Resolving Power, Resolution, and Collision Cross Section: Unifying Cross-Platform Assessment of Separation Efficiency in Ion Mobility Spectrometry. *Anal. Chem.* **2017**, *89* (22), 12176–12184. https://doi.org/10.1021/acs.analchem.7b02827.
(35) Silveira, J. A.; Ridgeway, M. E.; Laukien, F. H.; Mann, M.; Park, M. A. Parallel Accumulation for 100% Duty Cycle Trapped Ion Mobility-Mass Spectrometry. *Int. J. Mass Spectrom.* **2017**, *413*, 168–175. https://doi.org/10.1016/j.ijms.2016.03.004.
(36) Fernandez-Lima, F. A.; Kaplan, D. A.; Park, M. A. Note: Integration of Trapped Ion Mobility Spectrometry with Mass Spectrometry. *Rev. Sci. Instrum.* **2011**, *82* (12), 126106. https://doi.org/10.1063/1.3665933.
(37) COMMISSION REGULATION (EU) 2017/ 644 - of 5 April 2017 - Laying down Methods of Sampling and Analysis for the Control of Levels of Dioxins, Dioxin-like PCBs and Non-Dioxin-like PCBs in Certain Foodstuffs and Repealing Regulation (EU) No 589 / 2014. *J Eur Union L* **2017**, *92*, 9–34.
(38) Working Group for Measurement Uncertainty in PCDD/F and PCB Analysis. Guidance Document on Measurement Uncertainty for Laboratories Performing PCDD/F and PCB Analysis Using Isotope Dilution Mass Spectrometry. **2017**.
(39) COMMISSION REGULATION (EU) 2023/915 of 25 April 2023 on Maximum Levels for Certain Contaminants in Food and Repealing Regulation (EC) No 1881/2006. *J Eur Union L* **2023**, *119*, 103–157.
(40) Goscinny, S.; Joly, L.; De Pauw, E.; Hanot, V.; Eppe, G. Travelling-Wave Ion Mobility Time-of-Flight Mass Spectrometry as an Alternative Strategy for Screening of Multi-Class Pesticides in Fruits and Vegetables. *J. Chromatogr. A* **2015**, *1405*, 85–93. https://doi.org/10.1016/j.chroma.2015.05.057.
(41) Regueiro, J.; Negreira, N.; Berntssen, M. H. G. Ion-Mobility-Derived Collision Cross Section as an Additional Identification Point for Multiresidue Screening of Pesticides in Fish Feed. *Anal. Chem.* **2016**, *88* (22), 11169–11177. https://doi.org/10.1021/acs.analchem.6b03381.
(42) Hinnenkamp, V.; Klein, J.; Meckelmann, S. W.; Balsaa, P.; Schmidt, T. C.; Schmitz, O. J. Comparison of CCS Values Determined by Traveling Wave Ion Mobility Mass Spectrometry and Drift Tube Ion Mobility Mass Spectrometry. *Anal. Chem.* **2018**, *90* (20), 12042–12050. https://doi.org/10.1021/acs.analchem.8b02711.
(43) Belova, L.; Celma, A.; Van Haesendonck, G.; Lemière, F.; Sancho, J. V.; Covaci, A.; Van Nuijs, A. L. N.; Bijlsma, L. Revealing the Differences in Collision Cross Section Values of Small Organic Molecules Acquired by Different Instrumental Designs and Prediction Models. *Anal. Chim. Acta* **2022**, *1229*, 340361. https://doi.org/10.1016/j.aca.2022.340361.

(44) Belova, L.; Caballero-Casero, N.; Ballesteros, A.; Poma, G.; Van Nuijs, A. L. N.; Covaci, A. Trapped and Drift-tube Ion-mobility Spectrometry for the Analysis of Environmental Contaminants: Comparability of Collision Cross-section Values and Resolving Power. *Rapid Commun. Mass Spectrom.* **2024**, *38* (21), e9901. https://doi.org/10.1002/rcm.9901.

(45) Celma, A.; Sancho, J. V.; Schymanski, E. L.; Fabregat-Safont, D.; Ibáñez, M.; Goshawk, J.; Barknowitz, G.; Hernández, F.; Bijlsma, L. Improving Target and Suspect Screening High-Resolution Mass Spectrometry Workflows in Environmental Analysis by Ion Mobility Separation. *Environ. Sci. Technol.* **2020**, *54* (23), 15120–15131. https://doi.org/10.1021/acs.est.0c05713.

(46) Celma, A.; Ahrens, L.; Gago-Ferrero, P.; Hernández, F.; López, F.; Lundqvist, J.; Pitarch, E.; Sancho, J. V.; Wiberg, K.; Bijlsma, L. The Relevant Role of Ion Mobility Separation in LC-HRMS Based Screening Strategies for Contaminants of Emerging Concern in the Aquatic Environment. *Chemosphere* **2021**, *280*, 130799. https://doi.org/10.1016/j.chemosphere.2021.130799.

(47) Gabelica, V.; Marklund, E. Fundamentals of Ion Mobility Spectrometry. *Curr. Opin. Chem. Biol.* **2018**, *42*, 51–59. https://doi.org/10.1016/j.cbpa.2017.10.022.

(48) Zheng, X.; Dupuis, K. T.; Aly, N. A.; Zhou, Y.; Smith, F. B.; Tang, K.; Smith, R. D.; Baker, E. S. Utilizing Ion Mobility Spectrometry and Mass Spectrometry for the Analysis of Polycyclic Aromatic Hydrocarbons, Polychlorinated Biphenyls, Polybrominated Diphenyl Ethers and Their Metabolites. *Anal. Chim. Acta* **2018**, *1037*, 265–273. https://doi.org/10.1016/j.aca.2018.02.054.

(49) Menger, F.; Celma, A.; Schymanski, E. L.; Lai, F. Y.; Bijlsma, L.; Wiberg, K.; Hernández, F.; Sancho, J. V.; Ahrens, L. Enhancing Spectral Quality in Complex Environmental Matrices: Supporting Suspect and Non-Target Screening in Zebra Mussels with Ion Mobility. *Environ. Int.* **2022**, *170*, 107585. https://doi.org/10.1016/j.envint.2022.107585.

(50) Palm, E. H.; Engelhardt, J.; Tshepelevitsh, S.; Weiss, J.; Kruve, A. Gas Phase Reactivity of Isomeric Hydroxylated Polychlorinated Biphenyls. *J. Am. Soc. Mass Spectrom.* **2024**, *35* (5), 1021–1029. https://doi.org/10.1021/jasms.4c00035.

(51) *Mass Spectrometry in Food and Environmental Chemistry*; Picó, Y., Campo, J., Eds.; The Handbook of Environmental Chemistry; Springer International Publishing: Cham, 2023; Vol. 119. https://doi.org/10.1007/978-3-031-19093-3.